Effect of Na_2O on Viscosity, Structure and Crystallization of $CaF_2−CaO−Al_2O_3−MgO−TiO_2$ Slag in Electroslag Remelting

Jian-tao Ju[a, b, *], **Kang-shuai Yang**[a], **Yue Gu**[a], **and Kun He**[a]

[a] School of Metallurgical Engineering, Xi'an University of Architecture and Technology, Xi'an, 710055 China
[b] Shaanxi Engineering Research Center of Metallurgical, Xi'an, 710055 China
*e-mail: ju_jiantao@163.com

Abstract—The effect of Na_2O on the viscosity, structure, and crystallization behavior of $CaF_2−CaO−Al_2O_3−MgO−TiO_2$ slag was studied using the rotating cylinder method, differential scanning calorimetry, Fourier transform infrared spectroscopy, and X-ray diffraction analyses. The analyses demonstrated that with increasing Na_2O content, the viscosity and melting temperature of the slag decreased; however, the crystallization temperature increased. Na_2O acted as a network modifier to decrease the degree of polymerization in the titanoaluminate structure and consequently increased the mobility of ions in the slag structure. The network structures in the $[AlO_nF_{4-n}]$-tetrahedral complexes and $[AlO_4]$-tetrahedra are depolymerized with the addition of Na_2O; however, the depolymerization had a minimal effect on the Ti−O stretching vibration. During the continuous cooling process of the slag without Na_2O, the crystalline phases of $11CaO·7Al_2O_3·CaF_2$ were dominant, followed by CaF_2 and $CaTiO_3$. In addition to the first three phases, a new precipitated phase of $NaAlO_2$ was observed in the slag when Na_2O was added, and the sequence of crystallized precipitation during the continuous cooling process was $11CaO·7Al_2O_3·CaF_2$, CaF_2, $CaTiO_3$, and $NaAlO_2$. The effective activation energy of $11CaO·7Al_2O_3·CaF_2$ increased with increase in Na_2O content (0−3.9 wt %) and reached a maximum; however, a further increase in Na_2O content (6.6 wt %) decreased the effective activation energy of $11CaO·7Al_2O_3·CaF_2$.

1. INTRODUCTION

Recently, electroslag remelting (ESR), used in steelmaking, has received considerable attention in the production of high-quality steel and alloys including nickel-based superalloy [1−4]. The viscosity of the molten slag is an important thermophysical property in ESR, significantly impacted the purification of the liquid metal, the interface reaction kinetics between the slag and liquid metal, and the formation of a suitable slag film between the mold and solidified shell [2, 5]. To remove the detrimental effects such as environmental pollution and operator health hazards caused by fluoride evaporation in the smelting process of high-fluoride slag [4], studying relatively low-fluoride slag and fluorine-free slag could meet the ESR process requirements. Based on the $CaF_2−CaO−Al_2O_3$ ternary basic slag system, a small amount of SiO_2, MgO, TiO_2 and alkali metal oxides of Na_2O and Li_2O are added to the slag to meet the requirements of the specific smelting process [6−8]. However, a decrease in the CaF_2 content of the slag leads to an increase in its viscosity and melting temperature, which is not conducive to operational stability and

ingot quality. Previous studies [9, 10] have reported that the addition of Na_2O to slag could reduce its melting temperature and viscosity. However, limited research has been conducted on the fundamental physical properties of the relatively low-fluoride slag used for nickel-based superalloys. Therefore, studying the effect of Na_2O on the basic physical properties of slags, such as viscosity, melting temperature, and crystallization is essential.

Further, the viscosity of the slag is closely related to its structure [11]. Na_2O, as an alkali oxide, exists in the form of Na^+ and $O^{2−}$ ions, where the Na^+ ions are used for charge compensation and the $O^{2−}$ ions are used to alter the network structure. The combined effect of Na^+ and $O^{2−}$ ions on the slag structure leads to a corresponding variation in its basic physical and chemical properties. The influence of Na_2O on the viscosity and structure of slags has been reported. Kim et al. [10] observed that the slag viscosity decreased with increasing Na_2O content, and the Na^+ and $O^{2−}$ ions provided by Na_2O independently contributed to the depolymerization of the network structure of the molten slag. Jiang et al. [12] reported that the addition of

Table 1. Chemical composition of analytical reagents before and after pre-melting (wt %)

Sample	Before pre-melting						After pre-melting					
	CaF_2	CaO	Al_2O_3	MgO	TiO_2	Na_2O	CaF_2	CaO	Al_2O_3	MgO	TiO_2	Na_2O
N1	30.0	30.0	30.0	2.0	8.0	0.0	29.8	31.2	29.5	1.8	7.7	0.0
N2	30.0	28.5	28.5	2.0	8.0	3.0	28.9	30.9	28.6	1.7	7.5	2.4
N3	30.0	27.0	27.0	2.0	8.0	6.0	27.5	31.3	27.4	1.9	8.0	3.9
N4	30.0	25.5	25.5	2.0	8.0	9.0	26.9	30.9	25.9	1.9	7.8	6.6

Na_2O reduced the degree of the structural complexity of the slag by BO to Ti, NBO, and FO by means of molecular dynamics simulation, and increased the self-diffusion coefficients of each component of the slag system. The total self-diffusion coefficient of the slag system increased, which led to a decrease in slag viscosity. Their study predominantly focused on the slag viscosity and structure of aluminosilicates with different Na_2O contents. To prevent the reaction between SiO_2 in the slag with strong oxidizing alloying elements such as Al and Ti in liquid metal, SiO_2 is eliminated by adding an appropriate amount of TiO_2 and Ti burning loss is impeded [7]. A small amount of TiO_2 can decrease the viscosity and melting temperature, improve slag crystallization behavior [13, 14], and simplify the aluminate structure. However, the contribution of Na_2O to titanoaluminate structural changes in CaF_2–CaO–Al_2O_3–MgO—TiO_2-type ESR slags is yet to be discerned. The crystallization characteristics of Na_2O are also discussed because its horizontal heat transfer and lubrication performance depend on the crystallization characteristics of the slag [7].

In this study, the effect of Na_2O on the viscosity and structure of ESR slag containing TiO_2 was investigated using the rotating cylinder method and Fourier-transform infrared (FTIR) spectroscopy. The melting temperature of the slag was measured experi-mentally using the hemisphere method. The crystallization behavior of ESR-type CaF_2–CaO–Al_2O_3–MgO—TiO_2 with different Na_2O contents was studied by differential scanning calorimetry (DSC) and X-ray diffraction (XRD) analyses.

2. EXPERIMENTAL SECTION

2.1. Sample Preparation

The slag samples were prepared using analytical reagents consisting of CaF_2, CaO, Al_2O_3, MgO, TiO_2, and Na_2CO_3, as listed in Table 1. All reagents were heated up to 200°C for 4 h to remove moisture, whereas the CaO powder was calcined at 1000°C for 4 h in a box furnace to remove impurities and moisture. Subsequently, the treated reagents used for each slag sample were mixed thoroughly in mortar for 30 min, respectively. The mixed reagents samples were pre-melted in Pt crucible in a box furnace at 1500°C for 5 min. Then, the molten slag was rapidly quenched by ice water, which had an amorphous pattern as identified using XRD (Fig. 1) and was used as the sample for further characterization. X-ray fluorescence (XRF) was used to determine the chemical composition after pre-melting, and the results are listed in Table 1.

2.2. Experimental Procedure

2.2.1. Viscosity measurement. The melting characteristics of the molten slag were observed to determine the upper temperature of the viscosity measurement, which is an important thermophysical characteristic in the ESR process. A melting temperature tester (CQKJ-II, Chongqing University of Science and Technology, Chongqing, China) was used to measure the characteristic temperatures of the slag. The detailed experimental procedure is provided in a paper published by the author [15].

Rotating cylinder method was used to measure the viscosity of the molten slag using an HRV-1600P viscometer (Sinosteel Luoyang Institute of Refractories Research Co., Ltd, Luoyang, China). A schematic of the viscosity device and the dimensions of the crucible are shown in Fig. 2 and Table 2, respectively. The viscosity device should be calibrated using standard castor oil with a known viscosity to obtain accurate results
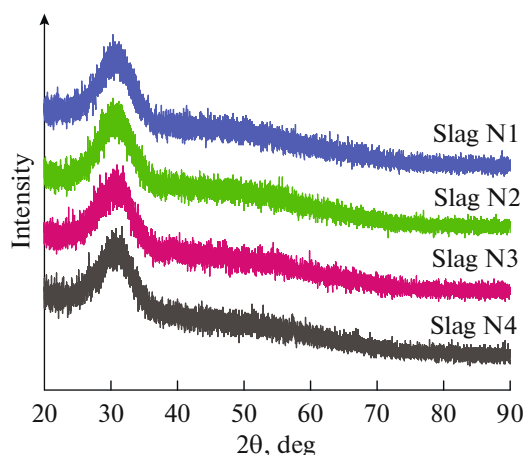
Fig. 1. XRD patterns of the slag samples.

before each viscosity measurement. The high purity graphite crucible with reagent samples was placed in a constant temperature zone in a pit furnace, heated up to 1550°C, and sustained for 10 min to ensure complete melting. The raising furnace body is aimed to ensure that Mo spindle was completely in the molten slag, and the viscosity was measured at a continuous cooling rate of 6°C/min. The computer automatically recorded the viscosity values at different temperatures, that is, the viscosity-temperature curve was plotted. In the viscosity measurement process, nitrogen (99.99%) was used as a protective gas to prevent the oxidation of the Mo spindle and graphite crucible.

2.2.2. DSC measurement. The non-isothermal crystallization characteristics of the quenched slag samples were measured by DSC analysis using a simultaneous thermal analyzer (STA449F3, Netzsch Instrument Inc., Hamburg, Germany). The apparatus was calibrated using an Ar gas atmosphere at 60 mL/min as a reference to build a temperature calibration curve. The slag sample (50 ± 0.5 mg) in the Pt crucible was heated in the range of 50−1500°C at a heating rate of 30°C/min and held for 1 min for uniform composition and bubble removal. Subsequently, the slag samples were cooled to 300°C at cooling rates of 15, 20, 25, and 30°C/min to obtain DSC curves. CCT diagrams of each slag were plotted using the DSC results.

2.2.3. Structural analysis. FTIR spectroscopy (Nicolet, Summit, USA) was used to determine the structural changes in the quenched slags. Prior to the measurement, the samples comprising 2.0 mg of premelted slag and 200 mg of KBr were pressed into discs of 13 mm in diameter using customized infrared tools. The FTIR spectra (32 scans per spectrum) were recorded in the range of 4000−400 cm^{-1} with a spectral resolution of 4 cm^{-1} at room temperature and collected using a KBr detector.

2.2.4. Crystalline phase analysis using XRD. Owing to the small amount of slag after the DSC measurement, a high-temperature furnace was used to determine the crystal precipitation species and sequence in the DSC measurements. The aforementioned treated analytical reagents were prepared as reagent samples, heated up to 1500°C for 5 min, and were cooled to the target temperature to obtain corresponding crystalline phases via rapid water cooling. In the high-temperature furnace, the cooling rate was set to 10°C/min, which was different from that in the DSC measurement (15°C/min). The pre-experiments showed that
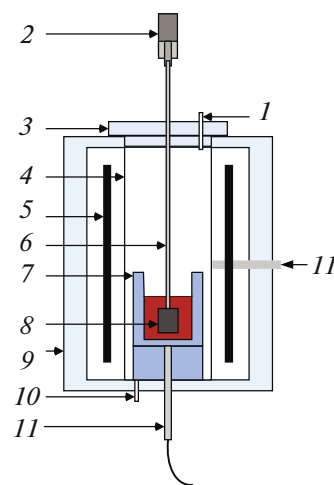

Fig. 2. Schematic of the experimental apparatus. (*1*) Gas outlet, (*2*) viscometer, (*3*) firebrick lid, (*4*) alumina tube, (*5*) MoSi$_2$ heating element, (*6*) shaft, (*7*) graphite crucible, (*8*) Mo spindle, (*9*) refractory, (*10*) gas inlet, and (*11*) B-type thermocouple.

the difference between the end-crystallization-temperature of a crystal in DSC and that of the high-temperature furnace was in the temperature range of −5 to −15°C. Therefore, to ensure that the crystalline phase could be precipitated, the crystallization temperature selected in the high-temperature furnace was lesser than −5 to −15°C, compared to that of the DSC measurement. The crystallization temperature used in the high-temperature furnace can be corrected according to the deviation of the pre-experiment. The crystalline phases were identified using XRD, and the sequence of the crystal phases was obtained by comparing different XRD curves at the target temperature for each sample.

3. RESULTS AND DISCUSSION

3.1. Effect of Na$_2$O on the Melting Characteristics of the Slag

To develop a lower-melting-point-slag system suitable for nickel-based superalloys, the process following the addition of Na$_2$O to CaF$_2$−CaO−Al$_2$O$_3$−MgO−TiO$_2$ slag was studied. The characteristic temperatures of slags with different Na$_2$O contents are listed in Table 3. Generally, the hemispherical temperature is regarded as the melting temperature of the slag. As the Na$_2$O contents increased from 0 to 6.6 wt %,

Table 2. Dimensions of the graphite crucible and spindle (mm)

Graphite crucible	Size	Mo Spindle	Size
Inner diameter	50	Diameter	15
Outer diameter	60	Height	20
Height	80	Submerged length	20

Table 3. Slag melting characteristics

Sample	Softening temperature, °C	Hemispheric temperature, °C
N1	1413	1468
N2	1375	1441
N3	1350	1424
N4	1335	1412

Table 4. Viscosity of the molten slags at 1550°C and break temperature

Sample	Viscosity at 1550°C (Pa s)	Break temperature, °C
N1	0.212	1457
N2	0.158	1432
N3	0.098	1414
N4	0.057	1392

the melting temperature gradually decreased from 1468 to 1412°C. Therefore, increasing the Na_2O content reduces the melting temperature of the slag, which follows the conclusions of a previous study [16]. In addition, Na_2O can also be a potential substitute for CaF_2 in the design of new ESR slags.

3.2. Effect of Na₂O on Viscosity

The temperature dependence of the viscosity in the $CaF_2-CaO-Al_2O_3-MgO-TiO_2$ slags with different Na_2O contents is shown in Fig. 3. All the viscosity-temperature curves have critical point, which is considered as the break temperature of the molten slag

(Table 4). As the temperature of the molten slag gradually decreased from 1550°C, the viscosity first increased slightly, and then abruptly increased when the temperature was below the break temperature during continuous cooling. This is because, at higher temperatures, the slag has sufficient excess thermal energy to modify the network structure, and at lower temperatures, a large number of precipitated phases increase the resistance effect between viscous flows [17].

Furthermore, from the perspective of Na_2O addition in the slag, the viscosity of the molten slag at 1550°C decreases with an increase in Na_2O content from 0 to 6.6 wt %, and the break temperature also decreases from 1457°C to 1392°C, as given in Table 4. However, at high temperatures (1470°C−1550°C), the slag viscosity gradually decreased with increasing Na_2O content (Fig. 3b). From the perspective of ion theory, Na_2O acts as a basic oxide, providing Na^+ and O^{2-} ions. The Na^+ ions have a higher priority for the ionic charge compensation effect for the aluminate structure than Ca^{2+} and Mg^{2+} ions to complicate the structure through the strict order for the cations used in the charge compensation of the Al^{3+} ions [18]. However, O^{2-} ions depolymerize the bridging oxygen bonds in the titanoaluminate structure to form simpler non-bridging oxygen bonds [19, 20]. The increase in the Na_2O content decreased the slag viscosity, which indicates that the depolymerization effect by O^{2-} ions is more dominant than the charge compensation effect by Na^+ ions. Further, a study used molecular dynamics simulation to investigate the decrease in slag viscosity with the addition of Na_2O content because it ameliorates the total self-diffusion coefficient of the slag system [12]. Therefore, the decrease in the viscosity of the molten slag caused by Na_2O addition is closely related to the effect of Na^+ and O^{2-} ions on the network structure, as described in Section 3.3.
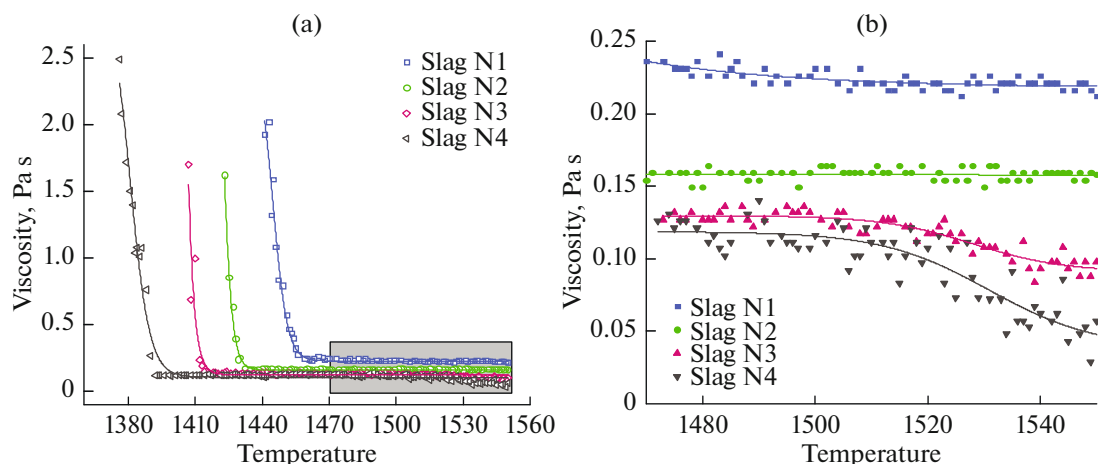
Fig. 3. Temperature dependence of viscosity in $CaF_2-CaO-Al_2O_3-MgO-TiO_2$ slag with different Na_2O contents.

3.3. Structural Analysis Using FTIR

To discern the relationship between the viscosity and the structure of the molten slag and to study the variation in the slag structure, FTIR spectra were recorded. The transmittance spectra of the CaF$_2$–CaO–Al$_2$O$_3$–MgO–TiO$_2$ slag with different Na$_2$O contents is shown in Fig. 4. The bands in the wavenumber range of 940–720 and 720–600 cm^{-1} are attributed to the asymmetric stretching vibration of [AlO$_n$F$_{4-n}$]-tetrahedral complexes ($n = 0$–4), [AlO$_4$]-tetrahedra, respectively [21]. Furthermore, the Ti–O stretching vibration was observed at approximately 420 cm^{-1} [22].

Increasing the addition of Na$_2$O content, shifts the center of gravity of [AlO$_n$F$_{4-n}$]-tetrahedral complexes toward lower wavenumbers, from 787 to 776 cm^{-1}. This shift indicates that the distance between cations and oxygen is broadened [10], that is, increasing the Na$_2$O content can depolymerize the network structure in the molten slag. The [AlO$_4$]-tetrahedra, generally occurring in the wavenumber range of 720–600 cm^{-1}, appears as a gentle slope near 660 cm^{-1} with low Na$_2$O content [20], which suggests a more complex network structure. Furthermore, the band at approximately 420 cm^{-1} is ascertained to the Ti–O stretching vibration, and the variation in its absorption intensity is significantly weak with an increase in Na$_2$O content. This suggests that increasing the Na$_2$O content had a minimal effect on the Ti–O bonds in the titanate structure.

Free oxygen (O^{2-}) reacts with bridge oxygens (O^0) to produce non-bridging oxygens (O$^-$) [9, 22, 23]. A shift in the center of gravity of [AlO$_n$F$_{4-n}$]-tetrahedral complexes toward lower wavenumbers with increasing Na$_2$O content indicates that Na$_2$O addition decreases the number of bridge oxygens and increases the number of non-bridge oxygens in the slag structure, resulting in simpler polymer-type units. The number of bridge oxygens in the [AlO$_4$]-tetrahedra also decreased with Na$_2$O addition. However, increasing the Na$_2$O content has a minimal effect on the Ti–O stretching vibration, which could be because the aluminate is dominant in the slag structure.

Based on the aforementioned structural analysis, the addition of Na$_2$O in the slag significantly depolymerized the [AlO$_n$F$_{4-n}$]-tetrahedral complexes and [AlO$_4$]-tetrahedra network structure, but only had a minimal effect on the Ti–O stretching vibration. The influence of O^{2-} ions provided by Na$_2$O addition on the titanoaluminate structure is more dominant than that of Na$^+$ ions. In addition, the complex network structure depolymerized by Na$_2$O addition is consistent with the result that viscosity decreases with increasing Na$_2$O content.
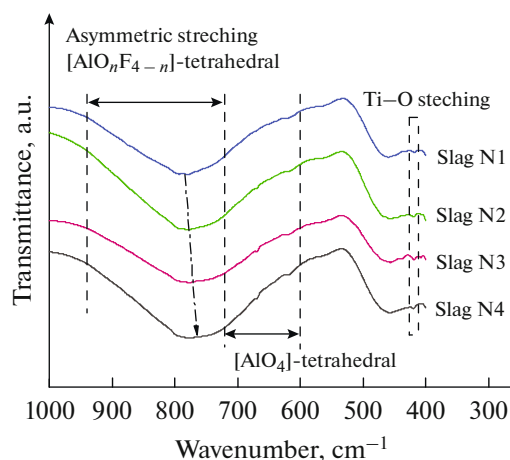

Fig. 4. FTIR spectra of the CaF$_2$–CaO–Al$_2$O$_3$–MgO–TiO$_2$ slag sample with different Na$_2$O contents, as-quenched at 1500°C.

3.4. DSC and XRD Analyses

The effect of Na$_2$O content on the DSC curves of slag samples with cooling rates of 15, 20, 25, and 30°C/min is shown in Fig. 5. Each exothermic peak represents a crystalline phase precipitated in the molten slag. Two crystallization events (T1 and T2) for Slag N1 and four crystallization events (P1, P2, P3, and P4) for Slag N2, Slag N3, and Slag N4 are observed in the DSC curves. Further, the crystallization of P1 is dominant in the slag containing Na$_2$O.

The XRD patterns of the quenched slags are shown in Fig. 6. The crystallization temperature of the samples was determined using the crystallization end temperature of each exothermic peak of the slags during the continuous cooling process. Two exothermic peaks, T1 and T2 appeared in the DSC curves for Slag N1 during the continuous cooling process; however, the corresponding XRD pattern has three crystalline phases. The exothermic peak, T1 represents the precipitation of 11CaO·7Al$_2$O$_3$·CaF$_2$ and that of T2 represents the precipitation of CaF$_2$ and CaTiO$_3$; this was confirmed by a similar result reported by Zheng et al. [14]. For the Slag N2, Slag N3, and Slag N4 slags with Na$_2$O content, a completely new crystalline phase was observed, which is attributed to the precipitation of NaAlO$_2$. The P1, P2, P3, and P4 exothermic peaks in the DSC curves of the slags were identified with reference to the corresponding XRD patterns; the peaks were ascertained to the crystalline phases of 11CaO·7Al$_2$O$_3$·CaF$_2$, CaF$_2$, CaTiO$_3$, and NaAlO$_2$, respectively. In addition, an increase in Na$_2$O addition promotes the precipitation of CaF$_2$ and NaAlO$_2$ crystalline phases, increasing the low-melting-point substances. This can be explained by the decreased break and melting temperatures of the molten slag with increasing Na$_2$O content.
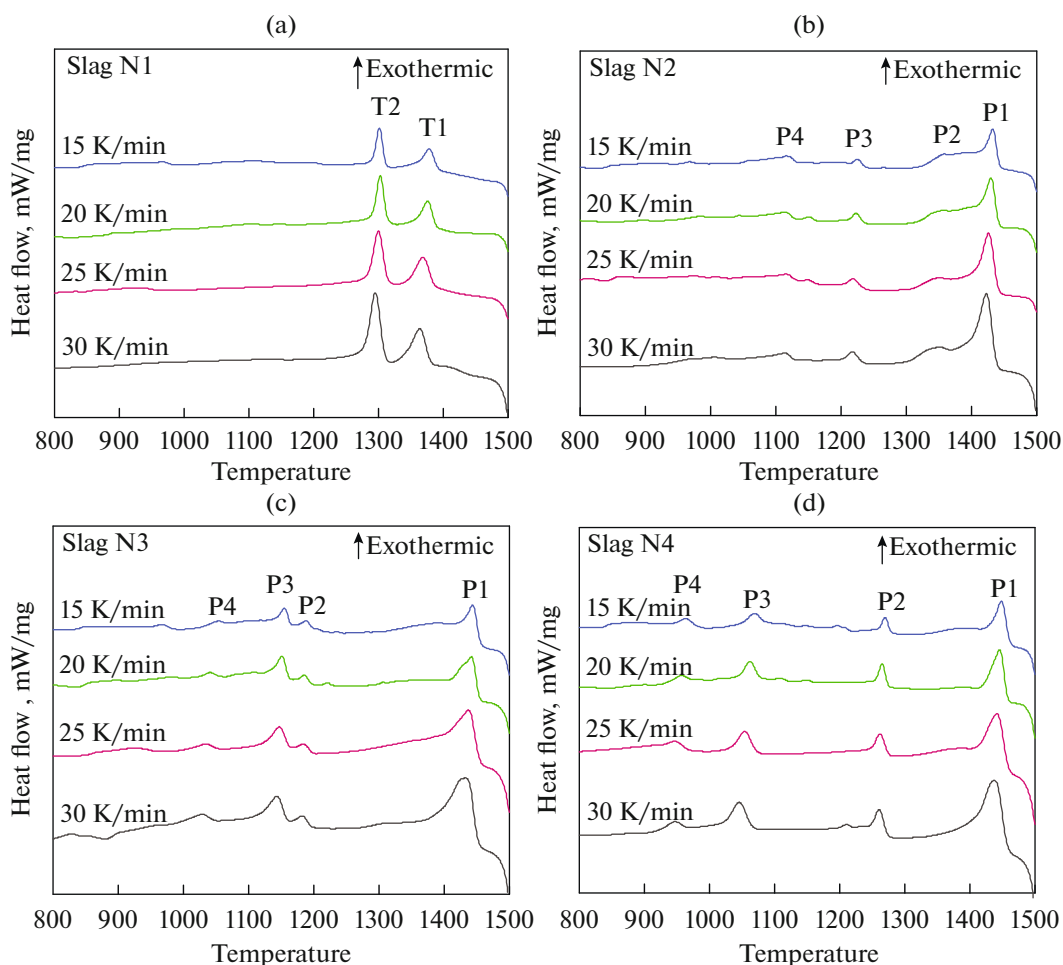
Fig. 5. DSC curves of non-isothermal crystallized molten slags at different rates: Slag N1 (a), Slag N2 (b), Slag N3 (c), and Slag N4 (d).

CCT diagrams of the crystalline phases of the slag are shown in Fig. 7 to discern their crystallization ability at different cooling rates of 15, 20, 25, and 30°C/min. The crystallization temperature of the crystalline phases of the molten slag decreases with an increase in cooling rate, indicating that a higher cooling rate represents a larger undercooling degree of the slag to a certain extent, resulting in a decrease in the onset crystallization temperature of the crystal. Additionally, a high cooling rate leads to a sharp increase in viscosity and produces a stronger driving force that accelerates molten slag nucleation [24].

The crystallization temperature of molten slag represents the temperature at which the initial crystalline phases are precipitated in successive non-isothermal crystallization processes [25]. The CCT diagram of the first crystalline phase precipitated in the molten slag is shown in Fig. 8. The increase in Na_2O contents increases in the crystallization temperature of the molten slags, when the continuous cooling rate is 15°C/min; the crystallization temperature of the molten slags corresponding to Na_2O content of 0, 2.4, 3.9,

and 6.6 wt % were 1398, 1448, 1463 to 1468°C, respectively. This result suggests that the crystallization temperature of the slag gradually increases. Previous studies have reported that Na_2O addition can increase the crystallization temperature of the slag and further promote its crystallization ability [24, 26, 27]. However, as the Na_2O content increased from 0 to 6.6 wt %, both the break temperature in the viscosity-temperature curve and the hemispheric temperature observed in melting properties by the hemispherical method decreased, which contradicts the tendency of the crystallization temperature in general. From the slag structural analysis, Na_2O acts as a network modifier to decrease the degree of polymerization in the titanoaluminate structure, resulting in a decrease in the melting and break temperatures, which reduces the relative resistance of the fluids [10, 28, 29]. In addition, the depolymerization effect facilitates the formation of much simpler polymers, which leads to an increase in the mobility of ions in the slag structure. Therefore, the addition of Na_2O enhances the crystallization of molten slag [16, 24].
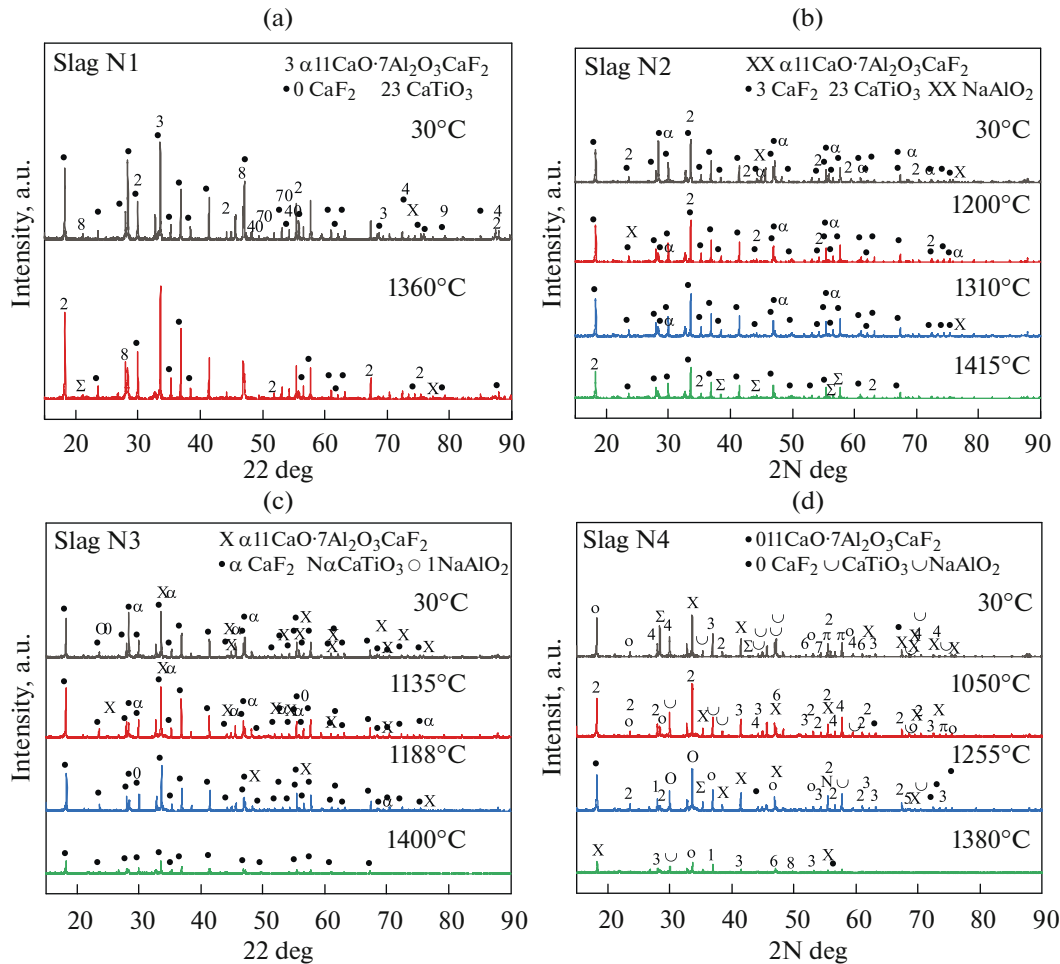
Fig. 6. XRD patterns of the molten slags, Slag N1 (a), Slag N2 (b), Slag N3 (c), and Slag N4 (d) at different rates.

3.5. Relative Crystallinity and Effective Activation Energy of $11CaO \cdot 7Al_2O_3 \cdot CaF_2$

Relative crystallinity is an important parameter for characterizing the structure of crystalline polymers, and it is closely related to many important properties of the polymer, such as the cooling rate, temperature, and effective activation energy. The equation for relative crystallinity is as follows:

$$\alpha(T) = \frac{\sum_{T_0}^{T}(dH/dT)dT}{\int_{T_0}^{T_e}(dH/dT)dT}, \quad (1)$$

where $\alpha(T)$ is the relative crystallinity at a certain temperature, and T, T_0, and T_e are the crystallization, onset, and end crystallization temperatures, respectively. dH/dT is the heat flow rate calculated from the first exothermic peak in the DSC curves.

The relative crystallinity of $11CaO \cdot 7Al_2O_3 \cdot CaF_2$ as a function of the crystallization time for various slag samples at different cooling rates is shown in Fig. 9. The relative crystallinity of $11CaO \cdot 7Al_2O_3 \cdot CaF_2$ gradually decreases with an increase in cooling rate for each quenched slag, indicating that increasing the cooling rate can shorten the crystallization time of the molten slag. Further, when the cooling rate is 15°C/min, the crystallization time of Slag N1 decreases significantly compared to that of Slags N2, N3, and N4, which indicates that the addition of Na₂O extends the crystallization time of the molten slag.

To discern the crystallization behavior of molten slag in terms of kinetics, the effective activation energy developed using a differential iso-conversional method for crystallization of molten slag, introduced by the Friedman method for non-isothermal crystallization kinetic analysis was utilized [30]. The effective activation energy is the temperature coefficient of the process rate, and it has a different physical meaning
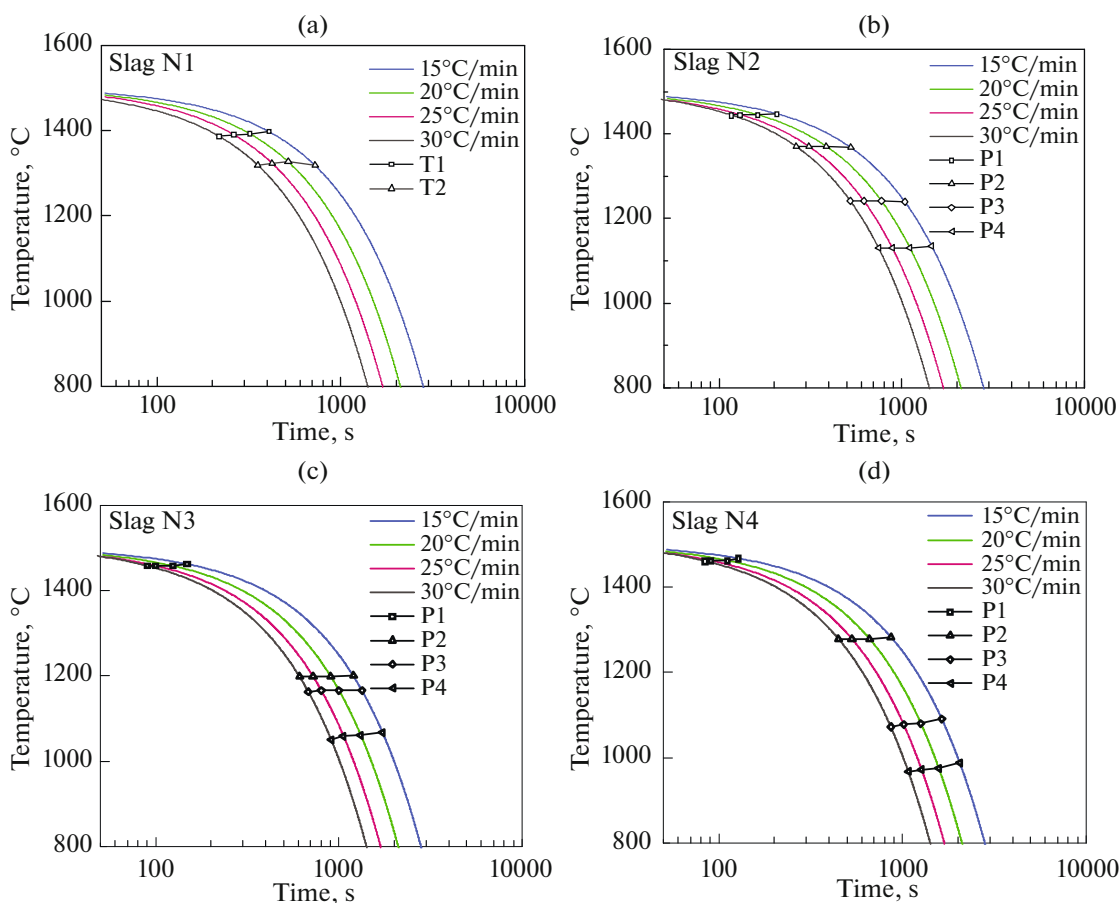
Fig. 7. CCT diagrams of the molten slags: Slag N1 (a), Slag N2 (b), Slag N3 (c), and Slag N4 (d).

from the apparent activation energy, which represents an energy barrier [31]. The equation is as follows:

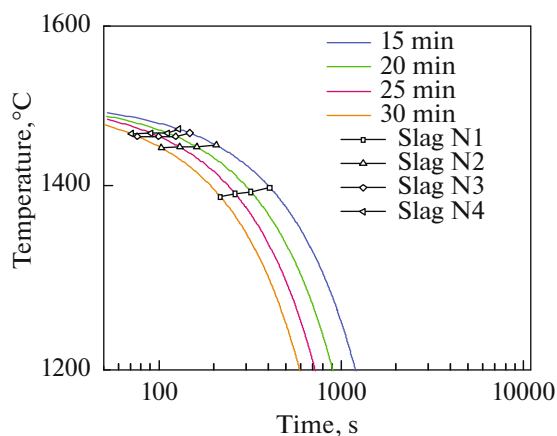$$\ln\left(\frac{d\alpha}{dt}\right) = -\frac{E_{c(\alpha)}}{RT_\alpha} + C, \qquad (2)$$

Fig. 8. CCT diagrams of the first crystalline phases precipitated in the molten slags.

where $d\alpha/dt$ is the instantaneous crystallization rate, and $E_{c(\alpha)}$, R, T_α, and C are the effect activation energy, gas constant, and temperature at the relative crystallinity α, respectively.

The effective activation energies for various slag samples under different relative crystallinities were calculated from the slope of the plot of the linear fitting of $\ln\left(\frac{d\alpha}{dt}\right)$ as a function of $-\frac{1}{RT_\alpha}$, for a series of given α values at different cooling rates. The effective activation energy of $11CaO\cdot7Al_2O_3\cdot CaF_2$ as a function of the relative crystallinity of the different slag samples is presented in Fig. 10. The effective activation energy of $11CaO\cdot7Al_2O_3\cdot CaF_2$ for Slag N1 first increased, then decreased, and finally increased again when the relative crystallinity increased, suggesting that the crystallization of $11CaO\cdot7Al_2O_3\cdot CaF_2$ was first inhibited, then enhanced, and finally inhibited again as the crystallization progressed. However, with increasing Na_2O addition, a successive increase in the effective activation energy of $11CaO\cdot7Al_2O_3\cdot CaF_2$ for Slag N2 and Slag N3 occurred, revealing that the crystallization of $11CaO\cdot7Al_2O_3\cdot CaF_2$ was restrained as the crys-
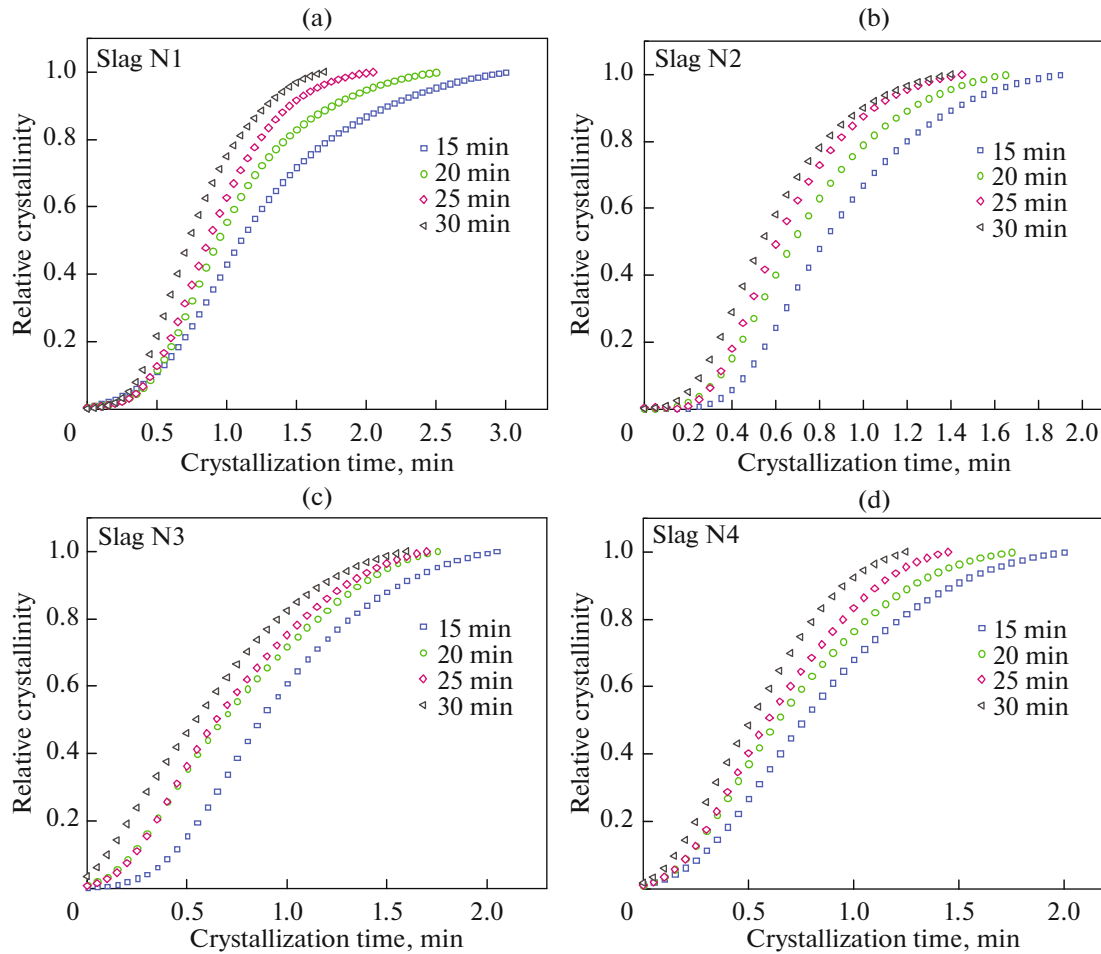
Fig. 9. Relative crystallinity of $11CaO \cdot 7Al_2O_3 \cdot CaF_2$ as a function of crystallization time for various slag samples at different cooling rates: Slag N1 (a), Slag N2 (b), Slag N3 (c), and Slag N4 (d).

tallization progressed. Considering the Na_2O addition with 6.6 wt %, the effective activation energy of $11CaO \cdot 7Al_2O_3 \cdot CaF_2$ for Slag N4 first increases and

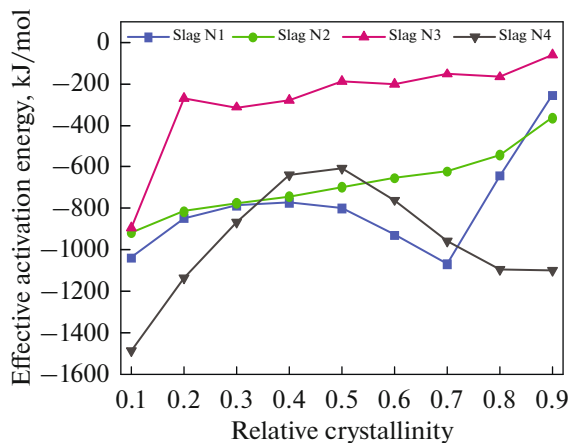**Fig. 10.** Effective activation energy of $11CaO \cdot 7Al_2O_3 \cdot CaF_2$ as a function of relative crystallinity for different slag samples.

then decreases, indicating that the crystallization of $11CaO \cdot 7Al_2O_3 \cdot CaF_2$ becomes easier and then harder. Further, the effective activation energy of $11CaO \cdot 7Al_2O_3 \cdot CaF_2$ increases with an increase in the Na_2O content from 0 to 3.9 wt %, however, a further increase in the Na_2O content decreases that of $11CaO \cdot 7Al_2O_3 \cdot CaF_2$.

4. CONCLUSIONS

The viscosity, structure, and crystallization behavior of $CaF_2-CaO-Al_2O_3-MgO-TiO_2$ slags with different Na_2O contents in ESR were studied using the rotating cylinder method, FTIR spectra, DSC, and XRD analysis. The conclusions are as follows:

As the Na_2O content increased from 0 to 6.6 wt %, the slag viscosity decreased from 0.212 to 0.057 Pa s, and the melting and breaking temperatures of the slag also decreased.

The $[AlO_nF_{4-n}]$-tetrahedral complexes and $[AlO_4]$-tetrahedra network structures were depolym-

erized by the addition of Na_2O, but they slightly affected the Ti—O stretching vibration. The O^{2-} ions generated by Na_2O on the titanoaluminate structure were more dominant than the Na^+ ions.

During the continuous cooling process of the slag without Na_2O, $11CaO \cdot 7Al_2O_3 \cdot CaF_2$ was first precipitated and was the dominant crystalline phase, followed by CaF_2 and $CaTiO_3$ together. Adding Na_2O to the slag leads to the production of a new precipitated crystalline phase of $NaAlO_2$, and the crystallization sequence of the slag is $11CaO \cdot 7Al_2O_3 \cdot CaF_2$, CaF_2, $CaTiO_3$, and $NaAlO_2$.

The crystallization temperature of the slag increases with the addition of Na_2O, which is because Na_2O plays the role of a network modifier to decrease the degree of polymerization in the titanoaluminate structure, facilitating the formation of simpler polymers and enhancing the mobility between ions in the slag structure. The effective activation energy of $11CaO \cdot 7Al_2O_3 \cdot CaF_2$ increases with an increase in Na_2O content from 0 to 3.9 wt %, but with a further increase in Na_2O contents, that of $11CaO \cdot 7Al_2O_3 \cdot CaF_2$ decreases.

CONFLICT OF INTEREST

The authors declare that they have no conflicts of interest.

REFERENCES

1. Shi, C.B., Deoxidation of electroslag remelting (ESR)—a review, *ISIJ Int.,* 2020, vol. 60, pp. 1083–1096.
https://doi.org/10.2355/isijinternational.ISIJINT-2019-661

2. Ju, J.T., Yang, K.S., Zhu, Z.H., and Gu, Y., Effect of CaF_2 and CaO/Al_2O_3 on viscosity and structure of TiO_2-bearing slag for electroslag, *J. Iron Steel Res. Int.,* 2021, vol. 28, pp. 1541–1550.
https://doi.org/10.1007/s42243-021-00683-2

3. Arh, B., Podgornik, B., and Burja, J., Electroslag remelting: A process overview, *Mater. Technol.,* 2016, vol. 50, pp. 971–979.
https://doi.org/10.17222/mit.2016.108

4. Xiong, Y.L., Song, Z.W., Wang, A.G., and Lou, Y.C., Factors influencing power consumption and power-saving measures in ESR process, *China Foundry,* 2019, vol. 16, pp. 1–7.
https://doi.org/10.1007/s41230-019-8135-5

5. Shi, C.B., Huang, Y., Zhang, J.X., Li, J., and Zheng, X., Review on desulfurization in electroslag remelting, *Int. J. Miner., Metall. Mater.,* 2021, vol. 28, pp. 18–29.
https://doi.org/10.1007/s12613-020-2075-3

6. Zheng, D.L., Li, J., Shi, C.B., and Ju, J.T., Effect of TiO_2 on the crystallization behaviour of CaF_2–CaO–Al_2O_3–MgO slag for electroslag remelting of Ti-containing tool steel, *Ironmaking Steelmaking,* 2016,

7. Shi, C.B., Li, J., Cho, J.W., Jiang, F., and Jung, I.H., Effect of SiO_2 on the crystallization behaviors and In-mold performance of CaF_2–CaO–Al_2O_3 slag for drawing-ingot-type electroslag remelting, *Metall. Mater. Trans. B,* 2015, vol. 46, pp. 2110–2120.
https://doi.org/10.1007/s11663-015-0402-2

8. Li, Q.H., Yang, S.F., Zhang, Y.L., An, Z.Q., and Guo, Z.C., Effect of MgO, Na_2O, and B_2O_3 on the viscosity and structure of Cr_2O_3-bearing CaO–SiO_2–Al_2O_3 slags, *ISIJ Int.,* 2017, vol. 57, pp. 689–696.
https://doi.org/10.2355/isijinternational.ISIJINT-2016-569

9. Li, W.L. and Xue, X.X., Effects of Na_2O and B_2O_3 addition on viscosity and electrical conductivity of CaO–Al_2O_3–MgO–SiO_2 system, *ISIJ Int.,* 2018, vol. 58, pp. 1751–1760.
https://doi.org/10.2355/isijinternational.ISIJINT-2018-212

10. Kim, H., Kim, W.H., Park, J.H., and Min, D.J., A study on the effect of Na_2O on the viscosity for iron-making slags, *Steel Res. Int.,* 2010, vol. 81, pp. 17–24.
https://doi.org/10.1002/srin.200900118

11. Wang, Q., Yang, J.A., Zhang, C., Cai, D.X., Zhang, J.Q., and Ostrovski, O., Effect of CaO/Al_2O_3 ratio on viscosity and structure of CaO–Al_2O_3-based fluoride-free mould fluxes, *J. Iron Steel Res. Int.,* 2019, vol. 26, pp. 374–384.
https://doi.org/10.1007/S42243-019-00248-4

12. Jiang, C.H., Zhang, H.X., Xiong, Z.X., Cheng, S., Li, K.J., Zhang, J.L., Liang, W., Sun, M.M., Wang, Z.M., and Wang, L., Molecular dynamics investigations on the effect of Na_2O on the structure and properties of blast furnace slag under different basicity conditions, *J. Mol. Liq.,* 2020, vol. 299, p. 112195.
https://doi.org/10.1016/j.molliq.2019.112195

13. Ju, J.T., Yang, K.S., Ji, G.H., Zhu, Z.H., and Liu, S.W., Effect of TiO_2 on viscosity and structure of low-fluoride CaF_2–CaO–Al_2O_3–MgO–Li_2O slag for electroslag remelting, *Rare Met. Mater. Eng.,* 2022, vol. 49, pp. 3676–3682.

14. Zheng, D.L., Li, J., Shi, C.B., and Ju, J.T., Crystallization characteristics and in-mold performance of electroslag remelting-type TiO_2-bearing slag, *Metall. Mater. Trans. B,* 2019, vol. 50, pp. 1148–1160.
https://doi.org/10.1007/s11663-019-01536-w

15. Ju, J.T., Ji, G.H., Tang, C.M., and An, J.L., Fluoride evaporation and melting characteristics of CaF_2–CaO–Al_2O_3–MgO–Li_2O–(TiO_2) slag for electroslag remelting, *Steel Res. Int.,* 2020, vol. 91, p. 2000111.
https://doi.org/10.1002/srin.202000111

16. Wang, Q., Yang, J., Zhang, J.Q., Ostrovski, O., Zhang, C., and Cai, D.X., Effect of Na_2O on properties, structure, and crystallization of CaO–Al_2O_3-based mold fluxes, *Steel Res. Int.,* 2022, vol. 93, p. 2100193.
https://doi.org/10.1002/srin.202100193

17. Kim, J.B. and Sohn, I., Influence of TiO_2/SiO_2 and MnO on the viscosity and structure in the TiO_2–MnO–SiO_2 welding flux system, *J. Non-Cryst. Solids,* 2013, vol. 379, pp. 235–243.
https://doi.org/10.1016/j.jnoncrysol.2013.08.010

18. Zhang, G.H., Chou, K.C., and Mills, K., A structurally based viscosity model for oxide melts, *Metall. Mater.*

vol. 45, pp. 135–144.
https://doi.org/10.1080/03019233.2016.1248699

Trans. B, 2014, vol. 45, pp. 698−706.
https://doi.org/10.1007/s11663-013-9980-z

19. Xu, R.Z., Zhang, J.L., Han, W.X., Chang, Z.Y., and Jiao, K.X., Effect of BaO and Na₂O on the viscosity and structure of blast furnace slag, *Ironmaking Steelmaking,* 2018, vol. 47, pp. 168−172.
https://doi.org/10.1080/03019233.2018.1498761

20. Kim, G.H. and Sohn, I., Influence of Li₂O on the viscous behavior of CaO−Al₂O₃−12 mass % Na₂O−12 mass % CaF₂ based slags, *ISIJ Int.,* 2012, vol. 52, pp. 68−73.
https://doi.org/10.2355/isijinternational.52.68

21. Park, J.H., Min, D.J., and Song, H.S., Structural investigation of CaO−Al₂O₃ and CaO−Al₂O₃−CaF₂ slags via Fourier transform infrared spectra, *ISIJ Int.,* 2002, vol. 42, pp. 38−43.
https://doi.org/10.2355/isijinternational.42.38

22. Zhang, Y.Y., Coetsee, T., Yang, H.F., Zhao, T., and Wang, C., Structural roles of TiO₂ in CaF₂−SiO₂−CaO−TiO₂ submerged arc welding fluxes, *Metall. Mater. Trans. B,* 2020, vol. 51, pp. 1947−1952.
https://doi.org/10.1007/s11663-020-01935-4

23. Sohn, I. and Min, D.J., A review of the relationship between viscosity and the structure of calcium-silicate-based slags in ironmaking, *Steel Res. Int.,* 2012, vol. 83, pp. 611−630.
https://doi.org/10.1002/srin.201200040

24. Li, J., Wang, W.L., Wei, J., Huang, D.Y., and Matsuura, H., A kinetic study of the effect of Na₂O on the crystallization behavior of mold fluxes for casting medium carbon steel, *ISIJ Int.,* 2012, vol. 52, pp. 2220−2225.
https://doi.org/10.2355/isijinternational.52.2220

25. Zheng, D.L., Li, J. and Shi, C.B., Development of low-fluoride slag for electroslag remelting: role of Li₂O on the crystallization and evaporation of the slag, *ISIJ Int.,* 2020, vol. 60, pp. 840−847.

https://doi.org/10.2355/isijinternational.ISIJINT-2019-575

26. Shu, Q.F., Klug, J.L., Medeiros, S.L.S., Heck, N.C., and Liu, Y., Crystallization control for fluorine-free mold fluxes: effect of Na₂O content on non-isothermal melt crystallization kinetics, *ISIJ Int.,* 2020, vol. 60, pp. 2425−2435.
https://doi.org/10.2355/isijinternational.ISIJINT-2020-132

27. Watanabe, T., Hashimoto, H., Hayashi, M., and Nagata, K., Effect of alkali oxides on crystallization in CaO−SiO₂−CaF₂ glasses, *ISIJ Int.,* 2008, vol. 48, pp. 925−933.
https://doi.org/10.2355/isijinternational.48.925

28. Xu, R.Z., Zhang, J.L., Han, W.X., Chang, Z.Y., and Jiao, K.X., Effect of BaO and Na₂O on the viscosity and structure of blast furnace slag, *Ironmaking Steelmaking,* 2020, vol. 47, pp. 168−172.
https://doi.org/10.1080/03019233.2018.1498761

29. Chang, Z.Y., Jiao, K.X., Ning, X.J., and Zhang, J.L., Novel approach to studying influences of Na₂O and K₂O additions on viscosity and thermodynamic properties of BF slags, *Metall. Mater. Trans. B,* 2019, vol. 50, pp. 1399−1406.
https://doi.org/10.1007/s11663-019-01565-5

30. Friedman, H.L., Kinetics of thermal degradation of char-forming plastics from thermogravimetry, *J. Polym. Sci., Part C: Polym. Symp.,* 1964, vol. 6, pp. 183−195.
https://doi.org/10.1002/polc.5070060121

31. Vyazovkin, S. and Sbirrazzuoli, N., Isoconversional analysis of the nonisothermal crystallization of a polymer melt, *Macromol. Rapid Commun.,* 2002, vol. 23, pp. 766−770.
https://doi.org/10.1002/1521-3927(20020901)23:13<766::AIMARC766>3.0.CO;2-0